Faraday Discussions

Accepted Manuscript

This manuscript will be presented and discussed at a forthcoming Faraday Discussion meeting. All delegates can contribute to the discussion which will be included in the final volume.

Register now to attend! Full details of all upcoming meetings: http://rsc.li/fd-upcoming-meetings

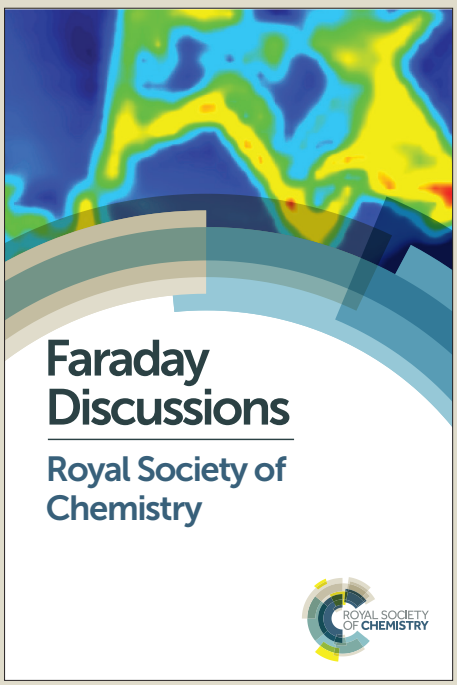

This is an *Accepted Manuscript*, which has been through the Royal Society of Chemistry peer review process and has been accepted for publication.

Accepted Manuscripts are published online shortly after acceptance, before technical editing, formatting and proof reading. Using this free service, authors can make their results available to the community, in citable form, before we publish the edited article. We will replace this *Accepted Manuscript* with the edited and formatted *Advance Article* as soon as it is available.

You can find more information about *Accepted Manuscripts* in the Information for Authors.

Please note that technical editing may introduce minor changes to the text and/or graphics, which may alter content. The journal's standard Terms & Conditions and the Ethical guidelines still apply. In no event shall the Royal Society of Chemistry be held responsible for any errors or omissions in this *Accepted Manuscript* or any consequences arising from the use of any information it contains.

ROYAL SOCIETY OF CHEMISTRY

www.rsc.org/faraday_d

Multifunctional Silica-Coated Iron Oxide Nanoparticles: A Facile Four-in-One System for In-Situ Study of Neural Stem Cells Harvesting

Yung-Kang Peng,[1⊥] C. N. P. Lui,[2⊥] Tsen-Hsuan Lin,[3] Chen Chang,[3] Pi-Tai Chou,[4] K.K. L. Yung[2] and S.C. Edman Tsang[1]*

[1]Department of Chemistry, University of Oxford, Oxford OX1 3QR, UK

[2]Department of Biology, Hong Kong Baptist University, Kowloon Tong, Hong Kong (China)

[3]Institute of Biomedical Sciences, Academia Sinica, Taipei 115, Taiwan

[4]Department of Chemistry, National Taiwan University, Taipei 106, Taiwan

Corresponding Author: Prof. S.C.E Tsang (edman.tsang@chem.ox.ac.uk)

[⊥]These authors contributed equally to this work.

ABSTRACT

Neural stem cells (NSCs), which generate main phenotypes of nervous system, are multipotent cells and are able to differentiate into multiple cell types *via* external stimuli from environment. The extraction, modification and re-application of NSCs have thus attracted much attention and raised the hope of novel neural stem cell therapies and regenerative medicine. However, few studies have successfully identified the distribution of NSCs in a live brain and monitored corresponding extraction processes both *in-vitro* and *in-vivo*. To address those difficulties, in this study, multi-functional uniform nanoparticles comprising an iron oxide and a functionalized silica shell (Fe_3O_4@SiO_2(FITC)-CD133, FITC: a green emissive dye, CD133: anti-CD133 antibody) have been strategically designed and synthesized for use as probe nanocomposites that combine four-in-one functionality, i.e., magnetic agitation, dual imaging (both magnetic resonance and optical) and specific targeting. It is shown that these newly synthesized Fe_3O_4@SiO_2(FITC)-CD133 particles have clearly facilitated their versatility in various applications. (1) The magnetic core facilitates the capability for magnetic cells collection and T_2 magnetic resonance imaging. (2) The fluorescent FITC embedded in silica framework enables optical imaging. (3) CD133 anchored on the outermost surface is demonstrated to be capable of targeting neural stem cells for cells collection and bimodal imaging.

1. INTRODUCTION

Neural stem cells (NSCs) are multipotent cells which are capable of self-replicating and generating various phenotypes of nervous system.[1-3] Numerous studies suggested that a subpopulation of cells surrounding lateral ventricle (LV) and sub-ventricular zone (SVZ) is capable of producing neurons for olfactory bulb in adults.[4-6] Furthermore, it has been proposed that the long-term potentiation is induced by the proliferation of NSCs in the dentate gyrus of hippocampus during memory formation. These findings potentiate the use of adult NSCs as a therapeutic tool in neurological disorders.[5,6] However, isolation of neural stem cells from a live brain without slaughtering the donor has been a great challenge.

To circumvent those difficulties, we have recently introduced a novel, precise and safe method to detach and collect the NSCs from the ependymal lining in adult rodent brain *in situ*.[7] We used magnetic nanoparticles conjugated with anti-CD133 antibodies to selectively target on the CD133 positive NSCs. After incubation for 6 hours, the particles were shown to specifically bind to the target cells. The animals were then placed under a weak external rotational magnetic field generated from the magnetic stirrer plate for the detachment of the stem cells localized along the SVZ/LV. The extracted stem cells after culture were also demonstrated to be differentiated into different neuronal phenotypes. Unfortunately, at that time, we were unable to monitor the real time distribution of the nanoparticles in rat brain and the fate of these particles since the selective binding and removal of labels/cells from the ependymal linings of SVZ/LV by the magnetic particles could be dynamic in the rat body. An *in situ* observation technique is therefore necessary to understand the time course and distribution of targeted stem cells in the rat brain.

Magnetic resonance imaging (MRI) has received much attention over the past two decades as a technique for the clinical diagnosis owing to its high resolution, unlimited tissue penetration, and absence of

ionizing radiation.[8-10] Contrast agents such as superparamagnetic iron oxide (Fe_3O_4) nanoparticles (NPs) with high r_2 relaxivity can generate (dark) signal in the corresponding area compared to background that have been widely used in clinical imaging. Since the r_2 relaxivity is proportional to the net magnetization (M_z) of the Fe_3O_4 NPs, the larger M_z of Fe_3O_4 nanoparticle can give a stronger T_2-weighted enhancement. To expand its applications in biomedicine, the design of multifunctional Fe_3O_4 NPs has been intensively pursued in the last ten years.[11-14] For instance, multifunctional magnetic NPs, which can render functions such as targeting, therapy, optical and MR imaging, have been achieved in *in vivo* tumor theranostic applications.[15,16]

In this study, first of all, we synthesized hydrophobic Fe_3O_4 NPs *via* thermal decomposition (high temperature) of iron oleate precursor instead of hydrophilic co-precipitation method we used previously (room temperature).[7] Since the magnetization of Fe_3O_4 NPs depends much on its crystallinity, the higher the temperature Fe_3O_4 nanoparticle is synthesized the higher magnetization it possesses.[17] The harvesting of targeted cells and their corresponding T_2-weighted MR signal can thus both be improved. Secondly, in order to combine both MR and optical imaging in a single nanoparticle (important to follow the fate of the labeled particle), we also incorporated amine-functionalized fluorescein isothiocyanate (FITC) in silica shell during the sol-gel reaction of tetraethyl orthosilicate (TEOS). The outmost silica surface of the resulting product, Fe_3O_4@SiO_2(FITC), was further immobilized anti-CD133 antibodies for specific targeting. The final product, Fe_3O_4@SiO_2(FITC)-anti-CD133 antibody (abbreviated as Fe_3O_4@SiO_2(FITC)-CD133 hereafter), combines four functions in a single unit, i.e. (1) The magnetic core serves not only as magnet for magnetic cells collection but also provides the capability for T_2 magnetic resonance imaging. (2) The fluorescent FITC embedded in silica framework enables optical imaging. (3) CD133 anchored on the outermost surface is

shown to be capable of targeting neural stem cells. Finally, the Fe_3O_4@SiO_2(FITC)-CD133 is demonstrated to be versatile in monitoring the time course distribution and the collection process of targeted stem cells in a living rat brain.

2. EXPERIMENTAL DETAILS

Chemicals. 1-octadecene (technical grade, 90%, Acros), oleic acid (90%, Acros), iron chloride ($FeCl_3 \cdot 6H_2O$, 40 mmol, Aldrich, 98%), hexanol (98%, Acros), Triton X-100 (Acros), tetraethyl orthosilicate (98%, Acros), ammonium hydroxide (28-30 wt %, Fluka), triethoxysilane ($HSi(OEt)_3$, Alfa Aesar), 3-aminopropyltrimethoxysilane (APTMS, 95%, Acros), 3-Aminopropyltrimethoxysilane (APTES, 97%, Aldrich), fluorescein isothiocyanate isomer I (FITC, 90%, Aldrich), N-(3-dimethylaminopropyl)-N'-ethylcarbodiimide hydrochloride (EDC, Aldrich), N-hydroxysuccinimide (NHS, 98%+, Acros), hexane and isopropyl alcohol were used without further purification.

Fe_3O_4 Nanoparticles. Iron oxide nanoparticles (NPs) were prepared by the method developed by Park et al. with minor modifications.[18] Iron oleate precursor was prepared by the reaction of iron chloride and oleic acid in methanol under basic conditions. Typically, 1.24 g of the iron oleate was used and dissolved in 10 g of 1-octadecene. The mixture solution was degassed at 100°C in order to remove any moisture and oxygen. The reaction mixture was subsequently treated with a definitive temperature program. First of all, the solution was rapidly heated to 200°C at a rate of 5°C/min. The solution was then further heated to 300°C at a heating rate of 1.2°C/min with vigorous stirring and maintained at the temperature for 1 h before cooling to room temperature. Solid samples were collected via centrifuging at 9000 rpm for 3 min, washed, and then

redispersed the precipitate with hexane and isopropyl alcohol several times. Finally, the purified Fe_3O_4 nanoparticles were dried in the oven.

Fe_3O_4@SiO_2(FITC) Nanocomposites. The preconjugated N-1-(3-triethoxy-silylpropyl)-N-fluoresceyl thiourea (FITC-APTES) was prepared by combining 5 μL of APTES and 2 mL of 0.023 M FITC ethanolic solution under continuous stirring and dark conditions.[19] Fe_3O_4@SiO_2(FITC) nanocomposites were prepared from reverse micelles using a previously reported procedure.[20] The as-prepared Fe_3O_4 nanoparticles (see above) were used as seeds for growth of the SiO_2 shell. Briefly, Fe_3O_4 nanoparticles (2 mg), 100 μL of TEOS, and 100 μL of FITC-APTES ethanolic solution were added to a heterogeneous solution containing cyclohexane (24 mL), hexanol (4.8 mL), Triton X-100 (6 mL), and water (1 mL). After 6 h of stirring, NH_4OH (100 mL) was added to initiate the hydrolysis of both TEOS and FITC-APTES. Due to the $(EtO)_3Si$ functional groups on FITC-APTES, it is reasonable to expect the successful encapsulation of the small green-emitting FITC molecules by the SiO_2 shell. The reaction was allowed to continue for another 24 h with stirring at room temperature. The product, Fe_3O_4@SiO_2(FITC), was well dispersed in ethanol and was further purified by centrifugation.

Fe_3O_4@SiO_2(FITC)-CD133 Nanocomposites. For external coating the amino group on the surface of silica particles, 3-amino-propyltrimethoxysilane (10 μL) was added to a mixture of ethanol (30 mL), DI water (6 mL), NH_4OH (300 μL), and Fe_3O_4@SiO_2(FITC) (20 mg).[21] After 24 h, the sample was centrifuged several times to remove the unreacted chemicals. The precipitate of particles was then collected and redispersed in DI water. The anti-CD133 antibodies were covalently conjugated onto the silica coated magnetic nanoparticles by EDC/NHS chemistry.[7] Typically, Fe_3O_4@SiO_2(FITC)-NH_2 (16 mg) were incubated with 10 mg EDC and 10 mg NHS for 30 min. Then, anti-CD133 antibodies (1 mL) were added to the mixture and

incubated for 1 h at room temperature. The antibodies-conjugated Fe_3O_4@SiO_2(FITC) nanocomposites were purified by centrifugation at 10,000 rpm for 15 min and washed 3–4 times with PBS (pH 7.4).

Particle Characterization The shape and size distributions of the nanoparticles were measured with a JEOL JEM 1230 transmission electron microscope (TEM). Experiment of X-ray energy dispersive spectroscopy (EDS) was performed by using a GENESIS 2000 EDS detector connected to the TEM instrument. The conventional Formvar coated 200 mesh Cu grids were used for the above-mentioned electron microscope (EM) experiments. Powder X-ray diffraction data was collected on a Bruker D8 Advance diffractometer. The workup procedure was carried out with Cu Kr radiation (λ) 1.54178 Å. Magnetic measurements were performed by superconducting quantum interference device (SQUID) magnetometer (MPMS, Quantum Design). The measurements were recorded between −15000 and 15000 Oe at 300 K. The ζ-potential was measured in a Malvern Zetasizer 3000 HS. Suspensions (200 μg/mL) of each material DI water were prepared. The ζ-potential was measured immediately after ultrasonication for 5 min, and 10 scans were taken per sample. Measurements of r_1 and r_2 relaxation times were made at 40°C using a 0.47 T Minispec spectrometer (Bruker Minispec mq series relaxometer); r_2 relaxation times were determined using a CarrPurcellMeiboomGill (CPMG) sequence, recycle time 10 s, eight averages with phase cycling, and 180° pulse separation of 1 ms. Monoexponential fitting was performed to even echoes over 250 ms acquisition window. The r_1 relaxation was estimated using inversion recovery techniques, recycle time 10 s, four averages with phase cycling, and eight inversion times logarithmically spaced over the interval 0-2000 ms. Linear regression between r_1 and r_2 and iron concentration was performed using standard techniques.

In Vivo Experiments. Detail of the *in vivo* experimental procedures can be found in the supporting information and our previous report.[7] For *in vivo* MRI experiments, all animals were initially anesthetized

with 5% isoflurane at 1 L min^{-1} air flow. When fully anesthetized, the animal was placed in a prone position and fitted with a custom designed head holder inside the magnet. Isoflurane was then maintained with 1−1.5% for rat at 1 L·min^{-1} air flow throughout the experiments. Sprague−Dawley rat brain experiments were performed in a Biospec 4.7 T spectrometer before and at different times after the injection of Fe_3O_4@SiO_2(FITC)-CD133 with (T1/T2) TR = 500/5000 ms, (T1/T2) TEeff = 8/70 ms, FOV = 7 cm × 7 cm, slice thickness = 1.3 mm, and matrix size = 256 × 128 (zero-padded to 256 × 256) with six repetitions. Typically, nanoparticles suspended in PBS buffer (5 μL) were administrated stereotaxically into the SVZ/LV of the Institute of Cancer Research rats (8 weeks of age, male, body mass ~300 g) at a dose of 0.19 mg·kg^{-1}.

3. RESULTS AND DISCUSSION

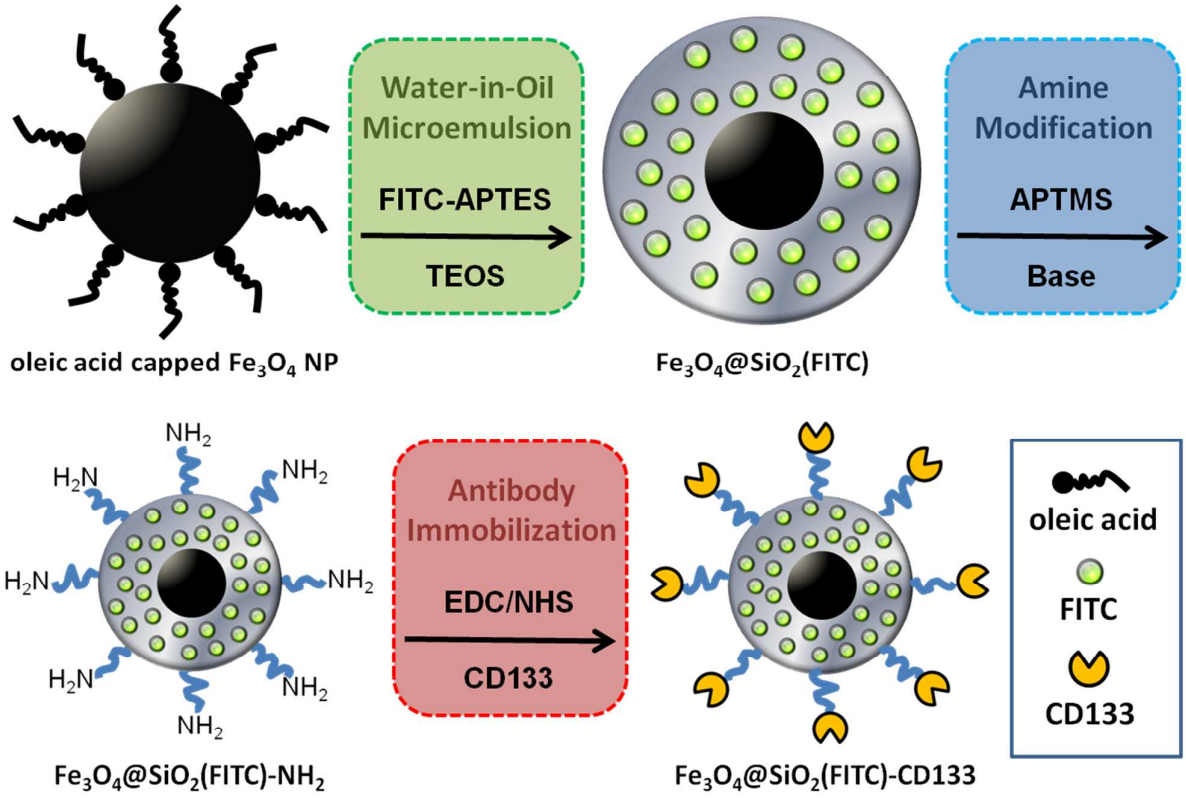

Scheme 1. Schematic illustration of the synthesis of Fe_3O_4@SiO_2(FITC)-CD133 nanocomposites.

Synthesis and characterization

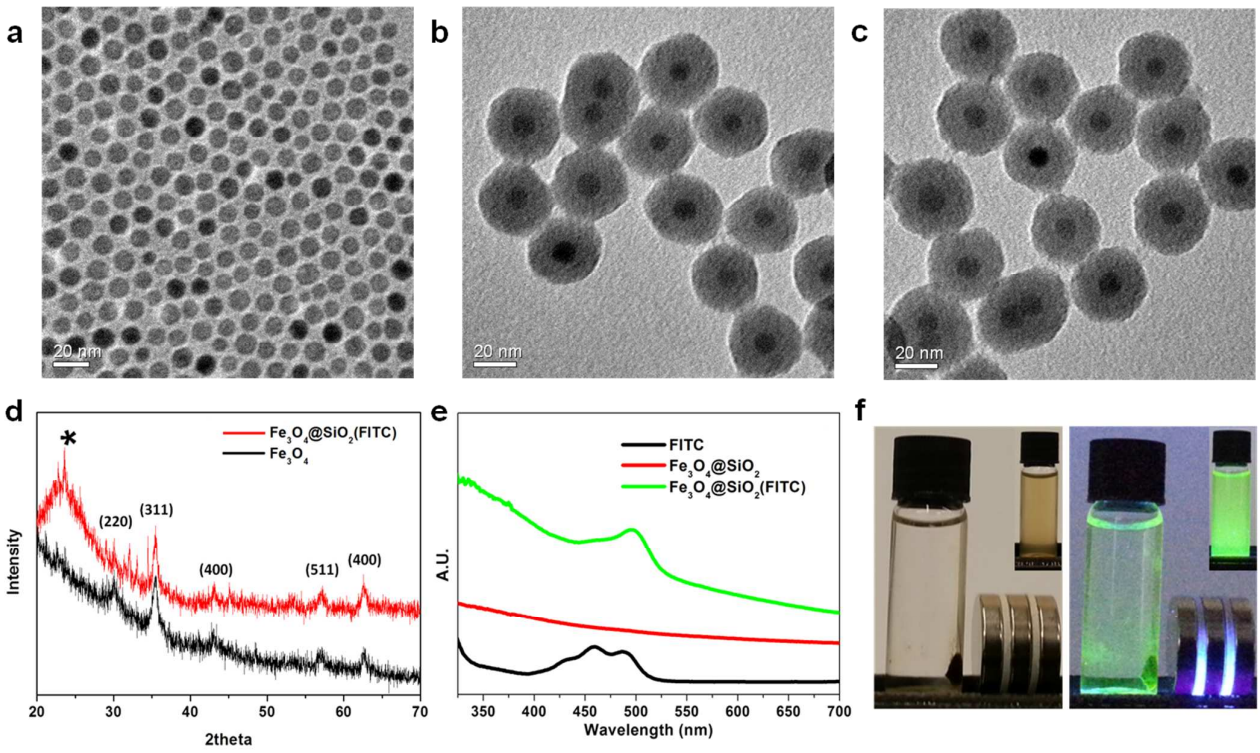

Figure 1. TEM of (a) oleic-acid-capped Fe_3O_4 NPs, (b) Fe_3O_4@SiO_2(FITC) and (c) Fe_3O_4@SiO_2(FITC)-CD133. (d) X-ray diffraction spectra of Fe_3O_4 NPs and Fe_3O_4@SiO_2(FITC). (e) Absorption spectra of FITC (black), Fe_3O_4@SiO_2 (red) and Fe_3O_4@SiO_2(FITC) (green). (f) The appearance of Fe_3O_4@SiO_2(FITC)-CD133 NPs upon placement of a magnet at one side of the vial (left) and the corresponding green emission produced under excitation by a 366-nm UV lamp (right). Inset: the appearance of the Fe_3O_4@SiO_2(FITC)-CD133 suspension in aqueous solution (left) and under UV excitation (right).

Scheme 1 illustrates the overall synthetic protocol (detail of the synthesis is described in the experimental section). First of all, the iron oxide NPs were synthesized by the thermal decomposition of precursor $Fe(oleate)_3$ complex in octadecene. As shown in Figure 1a, the oleic acid capped Fe_3O_4 NPs are nearly monodispersed ($\sigma < 7.5\%$) and well-dispersed. The average diameter is about 9.28±0.71 nm (50 particles are used for statistics) (Figure S1). Silica shell was then coated to the as-prepared Fe_3O_4 NP with a

sol-gel reaction of tetraethyl orthosilicate (TEOS) via a reverse micro-emulsion method. During the condensation reaction of TEOS, the amine functionalized fluorescence molecules N-1-(3-trimethyloxy-silylpropyl)-N'-fluoresceyl thiourea (APTES-FITC) can be encapsulated into the silica framework simultaneously. Because of the protection of the silica, the embedded fluorophores are expected to be stable against enzymatic digestion and thus rendering a long time cell tracking. Figure 1b shows the TEM image of the resulting product, Fe_3O_4@SiO_2(FITC), which possesses a homogeneous 10 nm silica shell around each Fe_3O_4 core. The average diameter of the nanocomposite is 31.71±1.54 nm (50 particles are used for statistics) (Figure S2). The corresponding XRD pattern (Figure 2d) confirms the existence of Fe_3O_4, and a broad peak around 23^o is attributed to the amorphous silica shell. The compositional verification of Fe_3O_4@SiO_2(FITC) nanocomposite was further analyzed by EDX spectroscopy (Figure S3) which confirms the existence of silicon, oxygen and iron elements. Both results (XRD and EDX) support that silica is successfully coated onto the Fe_3O_4 NP surface.

The coating mechanism of this water-in-oil microemulsion system has been studied recently.[22] It has been shown that the surfactant TritonX-100 not only forms micelles in the cyclohexane solution but also replaces the surfactant oleic acid once the Fe_3O_4 NPs are added. Later, the added TEOS will hydrolyze at the oil/water interface and perform the ligand exchange with TritonX-100 chemically absorbed on the Fe_3O_4 NPs surface and then transfer the NPs to the water phase. Finally, the hydrolyzed TEOS on the Fe_3O_4 NPs surface undergoes a condensation process and forms silica shells. In figure 1e, it is clear that the characteristic absorption bands at ~ 490 nm corresponding to the absorption of the FITC at significant quantity also appears in the Fe_3O_4@SiO_2(FITC) sample, while Fe_3O_4@SiO_2 shows no prominent absorption peak at this wavelength. Figure 1f demonstrates the magnetic separation of Fe_3O_4@SiO_2(FITC), for which

the green emission appears on the side of the magnet-adsorbed powder (figure 1f right), while there is no conspicuous emission remaining in solution, thus eliminating the existence of unencapsulated FITC. These results verify the successful encapsulation of FITC in silica framework.

The Fe_3O_4@SiO_2(FITC) NPs were then further modified with (3-aminopropyl)triethoxysilane (APTMS) under basic condition to yield Fe_3O_4@SiO_2(FITC)-NH_2 (scheme 1). It is believed that the triethoxysilane groups of APTMS can undergo condensation with hydroxyl groups on the outmost surface of Fe_3O_4@SiO_2(FITC) under basic condition, in which some hydroxyl groups would therefore be replaced by amine groups. Since the hydroxyl groups are negatively charged at neutral pH ($Si\text{-}O^-$), the modification of amine group (positive charged in neutral pH, NH_3^+) can be identified with zeta potential (ζ-potential) measurement.[23] As shown in figure S4, the value of ζ-potential for bare Fe_3O_4@SiO_2(FITC) increases positively from −44.5 mV (figure S4a) to −19.8 mV (figure S4b) after APTMS modification, suggesting the successful replacement of surface hydroxyl groups to amine groups. To render the core–shell particles with bio-targeting capability, antibodies CD133 were then conjugated with primary amine of Fe_3O_4@SiO_2(FITC)-NH_2 via an amide bond formation between the amine and the carboxylic acid of CD133. As shown in figure 1c, the final nanoparticles, Fe_3O_4@SiO_2(FITC)-CD133, remain well-shaped and no degradation of silica shell is observed after the amine and CD133 modification.

The magnetic properties of Fe_3O_4@SiO_2(FITC)-CD133 was assessed by superconducting quantum interference device (SQUID) (Figure S5). Compared to the magnetization value of naked Fe_3O_4 (~100 $emu\cdot g^{-1}$ at 300 K)[24], the magnitude for Fe_3O_4@SiO_2(FITC)-CD133 drops to ~70 $emu\cdot g^{-1}$, plausibly due to the introduction of the silica host and antibody CD133. However, the magnetization of Fe_3O_4@SiO_2(FITC)-CD133 is much higher than the previous one we used (~ 30 $emu\cdot g^{-1}$).[7] It should be

noted that the magnetic moment of the Fe_3O_4 NP is strongly dependent on the size, composition, and magneto-crystalline phase of the Fe_3O_4 NP.[17] Since both particle size and composition are comparable to our previous Fe_3O_4 NP (prepared by co-precipitation method), the high magnetization value achieved in this study should due to the high temperature preparation of Fe_3O_4 NP in oil phase, which provides its high crystallinity. The response of Fe_3O_4@SiO_2(FITC)-CD133 to external magnet was also demonstrated in figure 1f. On the other hand, as the transverse relaxivity (r_2) is strongly related to the net magnetization ($M_z \propto r_2$), the larger magnetization Fe_3O_4 nanoparticle has the stronger T_2-weighted enhancement it can provide. Figure S6 shows the corresponding longitudinal (r_1) and transverse relaxivity (r_2) of Fe_3O_4@SiO_2(FITC)-CD133 relaxation properties. The suppressed r_1 value (1.41 $mM^{-1}S^{-1}$), the high r_2 value (254.86 $mM^{-1}S^{-1}$) and the high r_2/r_1 ratio (as high as 180) clearly reveal that the nano-composite is a superior T_2 contrast agent.[17]

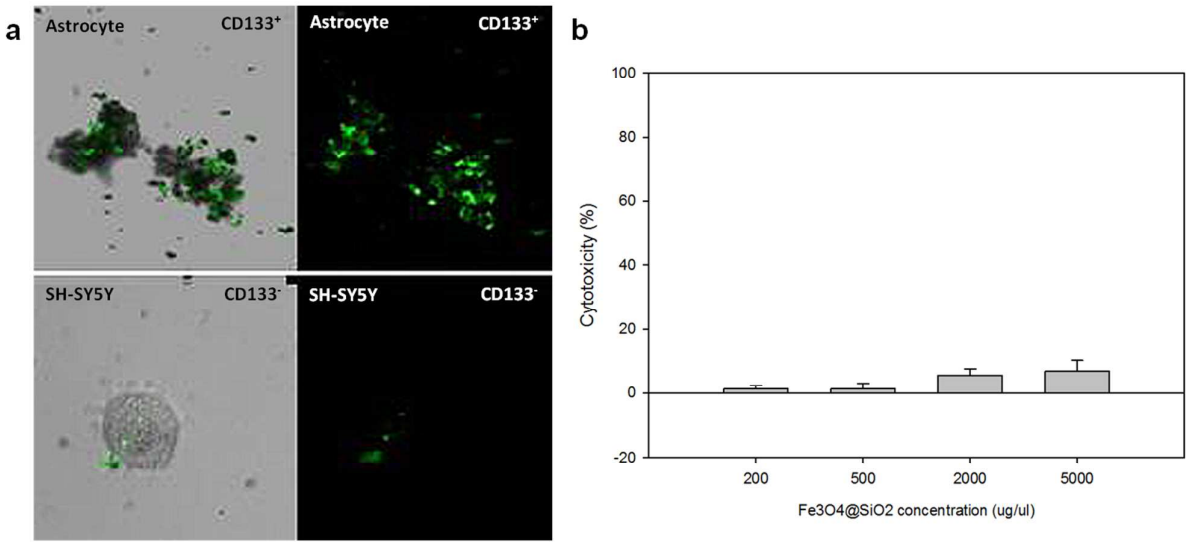

Figure 2. (a) Selective labelling of CD133 positive cells with Fe_3O_4@SiO_2(FITC)-CD133. The cells were incubated with particles for 6 hours *in vitro*. The Fe_3O_4@SiO_2(FITC)-CD133 can specifically bind onto (a) CD133 positive primary astrocytes (upper row) from PND 1 rats but not onto CD 133 negative SH-SY5Y cells (bottom row). (b) The LDH cytotoxicity assay illustrates that the percentage of cell death in CD133 positive primary astrocytes after 24 hours treatment with different concentrations of NPs ranging from 200 to 5000 μg/ml.

Since the Fe_3O_4@SiO_2(FITC)-CD133 should be able to selectively target for the CD133 positive neural stem cells, we therefore assessed the specificity of the Fe_3O_4@SiO_2(FITC)-CD133 particles by employing primary astrocytes ($CD133^+$) and SH-SY5Y cells ($CD133^-$) for an *in vitro* test. The distribution of Fe_3O_4@SiO_2(FITC)-CD133 in each cell solution was monitored by merging the differential interference contrast (DIC) (left column of figure 2a) and confocal images (right column of figure 2a). As shown in figure 2, the Fe_3O_4@SiO_2(FITC)-CD133 can favorably bind to the cell surface of the $CD133^+$ astrocytes. With a magnetic field applied to the cell culture, the $CD133^+$ cells tagged with Fe_3O_4@SiO_2(FITC)-CD133 could also be effectively driven in solution. While the CD133 negative SH-SY5Y cells were evenly distributed in the solution and the cells were immobilized on the application of a magnetic field.

Furthermore, lactate dehydrogenase (LDH) cytotoxicity assay was applied to assess the cytotoxicity of the NPs after 24 hr-exposure of the particles in the concentration range of 200-5000 μg/ml to $CD133^+$ astrocytes (figure 2b). The percentages of cell death were comparable among different groups and controls after the treatment. The as-prepared Fe_3O_4@SiO_2(FITC)-CD133 showed no sign of toxicity.

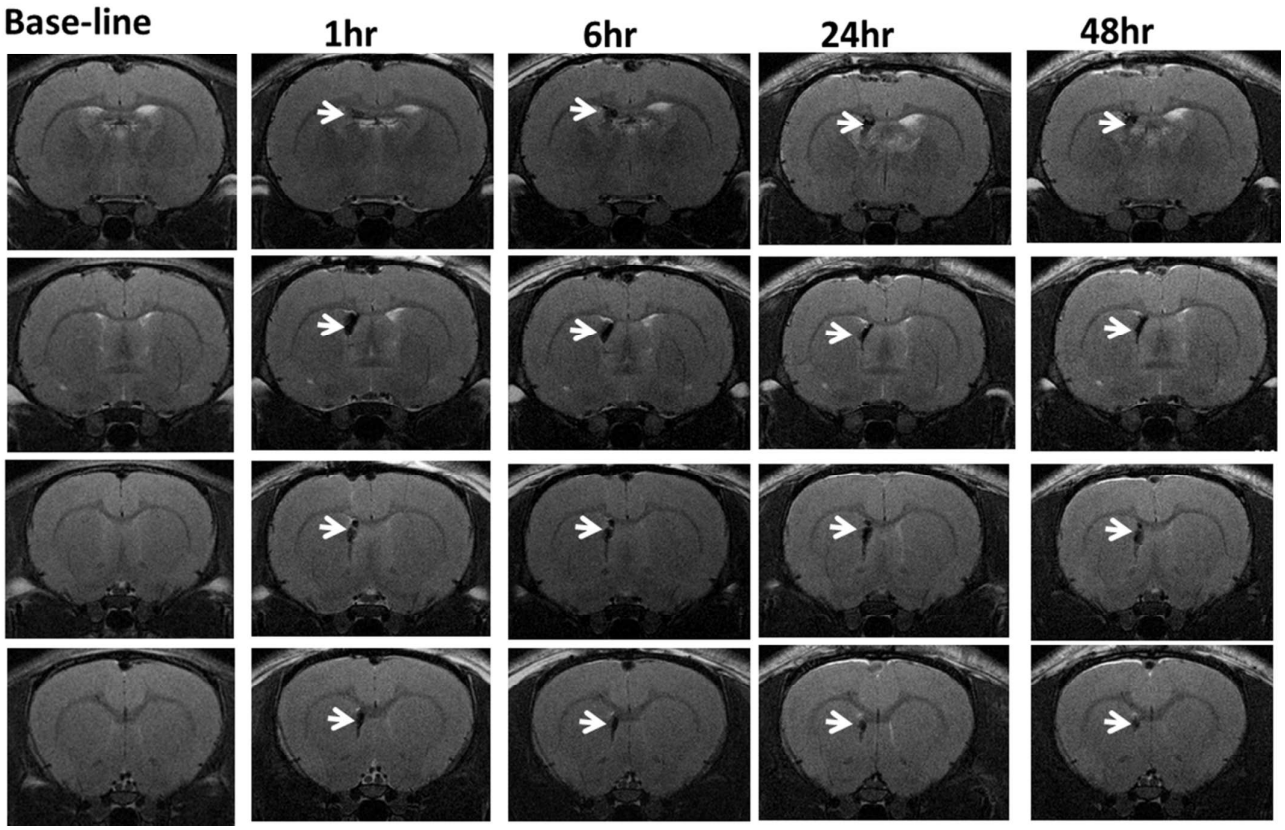

Figure 3. A spatial distribution (from posterior (row 1) to anterior (row 4), slice thickness = 1.3 mm) of T_2-weighted MR imaging of a rat brain (dark region) before and at different incubation times (1hr, 6hr, 24hr and 48hr) after injection of Fe_3O_4@SiO_2(FITC)-CD133.

To *in situ* study the time course distribution of injected Fe_3O_4@SiO_2(FITC)-CD133, we established an *in vivo* MR imaging of animal with a 4.7 T MR system. We have unilaterally injected the Fe_3O_4@SiO_2(FITC)-CD133 (2000 ug mL^{-1} in 5 mL of PBS) into the left ventricle of a live rat brain. It is envisaged that the Fe_3O_4@SiO_2(FITC)-CD133 would specifically bind to the NSCs. As shown in figure 3, the time course spatial distribution of the Fe_3O_4@SiO_2(FITC)-CD133 tagged NSCs could be monitored in real time without sacrificing the subjects. Coronal views of the T_2-weighted MRI images were acquired from posterior (row 1) to anterior (row 4) of the ventricles at different time points, i.e. 1 hour, 6 hours, 24 hours and 48 hours. The shape of left ventricle in T_2-weighted imaging became clear as we prolonged the

induction time from 1 hour to 48 hours. Figure S7 shows a time course of T_2 signal intensity of figure 3 row 3 (where we collected NSCs). Accordingly, the contrast to noise ratio (CNR) of the left ventricle reached to ~70% at the first hour administration with reference to the CNR before the administration. It is interesting to note that the highest contrast was indeed found on the SVZ/LV indicative of the preferential binding of the NSCs on this surface (no significant contrast was found in the fluid and other brain regions). In addition, the control experiment using the same particles but without the anti-CD133 antibodies did not seem to bind on the SVZ/LV region (but evenly distributed). This confirms our previous observation from using confocal microscopy that the labeled magnetic particles are mainly deposited on the choroid plexus lining along the SVZ/LV region.

It is thus believed that this contrast value of MRI reflected the amount of particles that can be rapidly attached on the surface containing the NSCs after the first hour of administration (excess particles in the fluid was quickly removed). However, this value declined to 60% at 6 hour and further dropped to ~40% after 24 hr incubation. Thus, the data clearly suggest some surface bound particles are unstable and can be continuously removed from the surface to the moving cerebrospinal fluid (CSF). In contrast, if we further prolonged the incubation time for another 24 hr, the SNR did not cause further decline (~48%) presumably the particles became strongly attached when the time progressed (or engulfed by the cells). This result indicates that the labels/cells on the ependymal lining of ventricle are rather dynamic, which can be flushed by the fluid or uptaken by the inner cells. Several processes should therefore be considered: (1) the diffusion and adsorption of particles on NSCs, (2) the removal of particles by CSF, (3) dynamically binding/(4) unbinding to NSCs and (5) the internalization of bound particles by NSC. Accordingly, the initial decrease of T_2 SNR signal can be attributed to the higher rate of particle removal (process 2 & 4) compared to the

counter processes (1), (3) and (5). However, the latter rates cannot be ignored as the time progresses further (figure S7). Based on the above discussion, the best operational time to monitor or extract the labeled surface region with NSCs should not be longer than 24 h after the administration otherwise nearly 50% of the particles would have been removed. In addition, the internalization of bound particles is rather significant at further prolonged times, such particles may not be detached to the fluid easily with or without applying external magnetic field. It should be noted here that no change of T_2 signal (no labeled particles in this region) was observed in the right ventricle throughout the whole studied period (figure S7). These results clearly indicate that (1) the particles could specifically bind to the CD133 positive cells on the left ventricle in alive subject and (2) the time for cells collection should be carried out within 24 hr incubation of Fe_3O_4@SiO_2(FITC)-CD133. It should be noted that the above conclusions are supported by our previous observation that a higher NSCs collection efficiency were actually found using a shorter induction time (6 h) than the longer induction time (24h) in the post-mortal analysis of the brain samples by confocal microscopy [7].

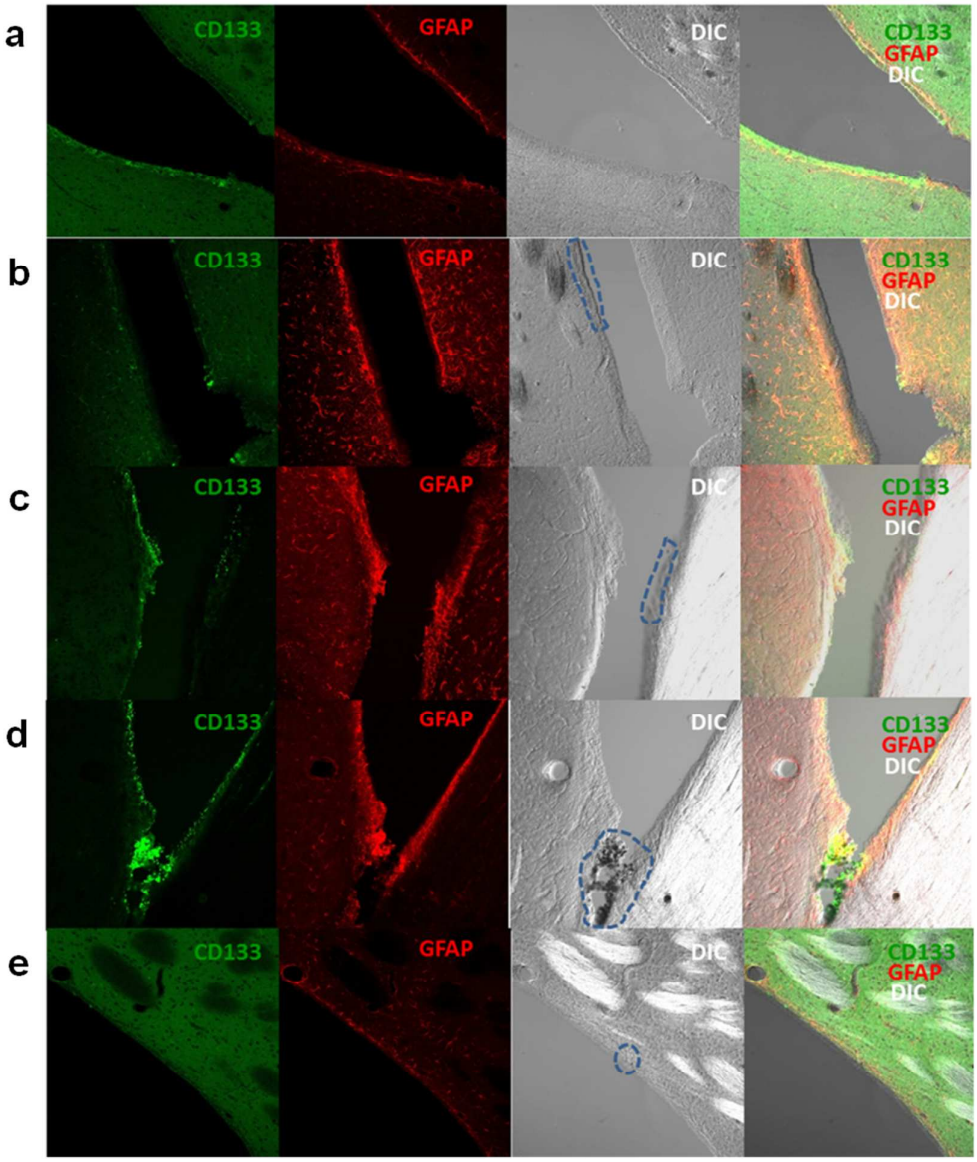

Figure 4. The efficiency of neural stem cell isolation with different magnetic agitation time is studied (a) 0 min; (b) 5 min; (c) 10 min; (d) 15 min with Fe_3O_4@SiO_2(FITC)-CD133 and (e) 15 min with Fe_3O_4@SiO_2(FITC). An effective detachment of the CD133 positive neural stem cells from the choroid plexus lining along the SVZ/LV can be found after 15-min agitation under a weak external rotational magnetic field. The dashed circles illustrate the presence of the nanoparticles.

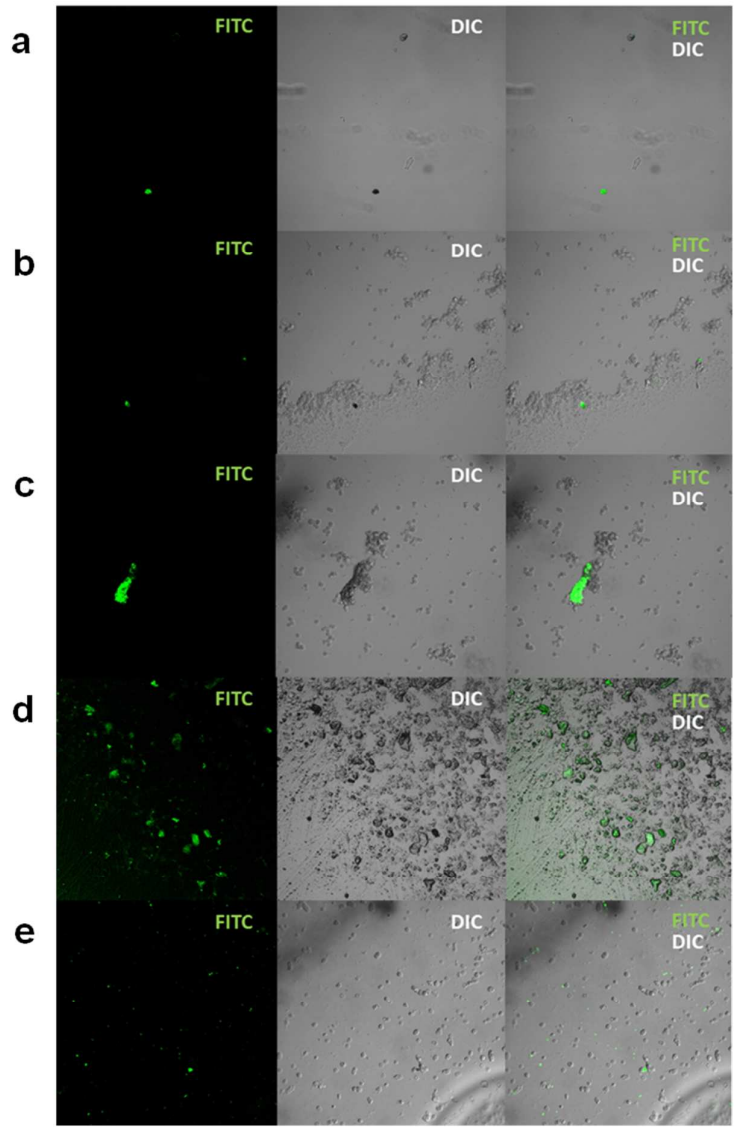

Figure 5. An *in vivo* extraction of CD133 positive neural stem cell is performed after magnetic agitation (a) 0 min; (b) 5 min; (c) 10 min; (d) 15 min with Fe_3O_4@SiO_2(FITC)-CD133 and (e) 15 min with Fe_3O_4@SiO_2(FITC). Around 1 ul of extract can be collected from subventricular zone/lateral ventricle by micro-syringe. The longer the agitation is, more CD133 postive cells can be isolated and collected for the further cell culture. Without the conjugation of antibody, the Fe_3O_4@SiO_2(FITC) can be found freely in the extract.

Besides evaluating the proper time events for these particles incubation by MRI, the magnetic agitation time to extract the bound NSCs using external magnetic field was also examined. The animals with the application of the labeled magnetic particles in left ventricles of their brains were then placed under a weak

external rotational magnetic field generated from a laboratory magnetic stirrer plate for the detachment of stem cells from the choroid plexus lining along the SVZ/LV. Notably, the duration of this "magnetic agitation" is thought to be critical for an efficient stem cells extraction. We have compared several agitation time (0 min, 5 min, 10 min and 15 min) and 15-min magnetic agitation was shown to be effectively isolated the neural stem cells from SVZ/LV (Figure 4 and 5) without inducing a great damage to the cells and linings. Our previous study also demonstrated the extracted cells could be collected for cell culture by a micro-syringe. The extracted stem cells were able to be cultured and further differentiated into different neuronal phenotypes *in-vitro*.[7] With all these promising findings, we propose that the patients could supply their own neural stem cells at some stage of their life expectancy for the later cells replacement treatments. The risk of immune rejection could be greatly reduced as the cells are all originated from the same individuals. An innovative tailor-made neurological disorder therapy by using the stem cells originated from the subjects themselves can thus be envisaged.

4. CONCLUSIONS

In summary, we demonstrate a biocompatible magnetofluorescent T_2 MRI contrast agent for targeted MR and fluorescence imaging of neural stem cells and their extraction based on silica-coated Fe_3O_4 NPs. This multifunctional nanoparticle, Fe_3O_4@SiO_2(FITC)-CD133 is shown to facilitate in-situ imaging and harvesting of the neural stem cells. (1) The magnetic core facilitates the capability for magnetic cell collection and T_2 magnetic resonance imaging. (2) The fluorescent FITC embedded in silica framework enables optical imaging. (3) anti-CD133 antibodies anchored on the outermost surface is shown to be capable of targeting neural stem cells for cells collection and bimodal imaging. The spatial distribution of T_2-weighted MR imaging of a rat brain clearly indicates that the binding/removal of labels/cells from the

ependymal linings of ventricle is dynamic and an incubation time is required for the elementary surface binding processes to reach equilibrium. The best operation time (to monitor or extract the labeled NSCs) should not be longer than 24 h otherwise nearly half of the particles would have been removed by the CSF. According to the MRI and optical data, our studies clearly show that the Fe_3O_4@SiO_2(FITC)-CD133 specifically targeted neural stem cells can be efficiently isolated by external magnetic agitation. Finally, it is also worth noting that the current technology for stem cells collection in a live brain may also be extended to other cells' extracts in particular areas of a subject by modifying corresponding targeting ligand on the outmost silica surface. Noticeably, the cells distribution and the process of cells extraction could also be monitored by the MRI and the optical imaging using the related particles prepared by the nano-chemistry as described above.

Acknowledgments

We thank the EPSRC of UK for initial funding of this project. YKP acknowledges the University of Oxford Clarendon Fund Scholarship for his DPhil study. We are indebted to the support from Taiwan Mouse Clinic which is currently funded through the National Research Program for Biopharmaceuticals (NRPB) at the National Science Council of Taiwan, particularly for the MRI mouse experiments presented in this paper.

References and Notes

1. F. Doetsch, I. Caille, D.A. Lim, J.M. Garcia-Verdugo and A. Alvarez-Buylla, *Cell* 1999, **97**, 703–716.
2. S. Pluchino, L. Zanotti, B. Rossi, E. Brambilla, L. Ottoboni, G. Salani, M. Martinello, A. Cattalini, A. Bergami, R. Furlan, G. Comi, G. Constantin and G. Martino, *Nature*, 2005, **436**, 266–271.
3. G.L. Ming and H.J. Song, *Neuron* 2011, **70**, 687–702.
4. C.B. Johansson, S. Momma, D.L. Clarke, M. Risling, U. Lendahl and J. Frisen, *Cell* 1999, **96** 25–34.

5. M. Carlen, K. Meletis, C. Goritz, V. Darsalia, E. Evergren, K. Tanigaki, M. Amendola, F. Barnabe-Heider, M.S.Y. Yeung, L. Naldini, *Nat. Neurosci.* 2009, **12**, 259–267.

6. L.C. Fuentealba, K. Obernier and A. Alvarez-Buylla, *Cell Stem Cell* 2012, **10**, 698–708.

7. C. N. P. Lui, Y. P. Tsui, C. T. Wu, A. S. L. Ho, D. K. Y. Shum, Y. S. Chan, H. W. Li, S. C. E. Tsang and K. K. L. Yung, *Angew. Chem. Int. Ed.* 2013, **52**, 12298–12302.

8. P. Caravan, J. J. Ellison, T. J. McMurry and R. B. Lauffer, *Chem. Rev.* 1999, **99**, 2293–2352.

9. P. Caravan, *Chem. Soc. Rev.* 2006, **35**, 512–523.

10. Y.-K. Peng, C.-L. Liu, H.-C. Chen, S.-W. Chou, W.-H. Tseng, Y.-J. Tseng, C.-C. Kang, J.-K. Hsiao and P.-T. Chou, *J. Am. Chem. Soc.* 2013, **135**, 18621–18628.

11. M. F. Kircher, U. Mahmood, R. S. King, R. Weissleder, L. *Cancer Res.* 2003, **63**, 8122–8125.

12. M. S. Martina, J. P. Fortin, C. Menager, O. Clement, G. Barratt, C. Grabielle-Madelmont, F. Gazeau, V. Cabuil and S. Lesieur, *J. Am. Chem. Soc.* 2005, **127**, 10676–10685.

13. C. W. Lai, Y. H. Wang, C. H. Lai, M. J. Yang, C. Y. Chen, P. T. Chou, C. S. Chan, Y. Chi, Y. C. Chen and J. K. Hsiao, *Small* 2008, **4**, 218–224.

14. Y. Chen, H. R. Chen, D. P. Zeng, Y. B. Tian, F. Chen, J. W. Feng and J. L. Shi, *ACS Nano* 2010, **4**, 529–539.

15. J. E. Lee, N. Lee, H. Kim, J. Kim, S. H. Choi, J. H. Kim, T. Kim, I. C. Song, S. P. Park, W. K. Moon and T. Hyeon, *J. Am. Chem. Soc.* 2010, **132**, 552–557.

16. C. R. Thomas, D. P. Ferris, J.-H. Lee, E. Choi, M. H. Cho, E. S. Kim, J. F. Stoddart, J.-S. Shin, J. Cheon and J. I. Zink, *J. Am. Chem. Soc.* 2010, **132**, 10623–10625.

17. Y.-W. Jun, J.-H. Lee and J. Cheon, *Angew. Chem. Int. Ed.* 2008, **47**, 5122–5135.

18. J. Park, K. An, Y. Hwang, J.-G. Park, H.-J. Noh, J.-Y. Kim, J.-H. Park, N.-M. Hwang and T. Hyeon, *Nat. Mater.* 2004, **3**, 891–895.

19. Y.-S. Lin and C. L. Haynes, *Chem. Mater.* 2009, **21**, 3979–3986.

20. Y.-K. Peng, C.-W. Lai, C.-L. Liu, H.-C. Chen, Y.-H. Hsiao, W.-L. Liu, K.-C. Tang, Y. Chi, J.-K. Hsiao, K.-E. Lim, H.-E. Liao, J.-J. Shyue and P.-T. Chou, *ACS Nano*, 2011, **5**, 4177–4187.

21. M.-L. Ho, J.-M. Hsieh, C.-W. Lai, H.-C. Peng, C.-C. Kang, I-C. Wu, C.-H. Lai, Y.-C. Chen and P.-T. Chou, *J. Phys. Chem. C* 2009, **113**, 1686–1693.

22. H. L. Ding, Y. X. Zhang, S. Wang, J. M. Xu, S. C. Xu and G. H. Li, *Chem. Mater.* 2012, **24**, 4572–4580.

23. Y.-K. Peng, C.-W. Lai, Y.-H. Hsiao, K.-C. Tang and P.-T. Chou, *Mater. Express* 2011, **1**, 136−143.

24. J.-H. Lee, Y.-M. Huh, Y.-W. Jun, J.-W. Seo, J.-T. Jang, H.-T. Song, S. Kim, E.-J. Cho, H.-G. Yoon, J.-S. Suh and J. Cheon, *Nat. Med.* 2007, **13**, 95−99.

Supporting information

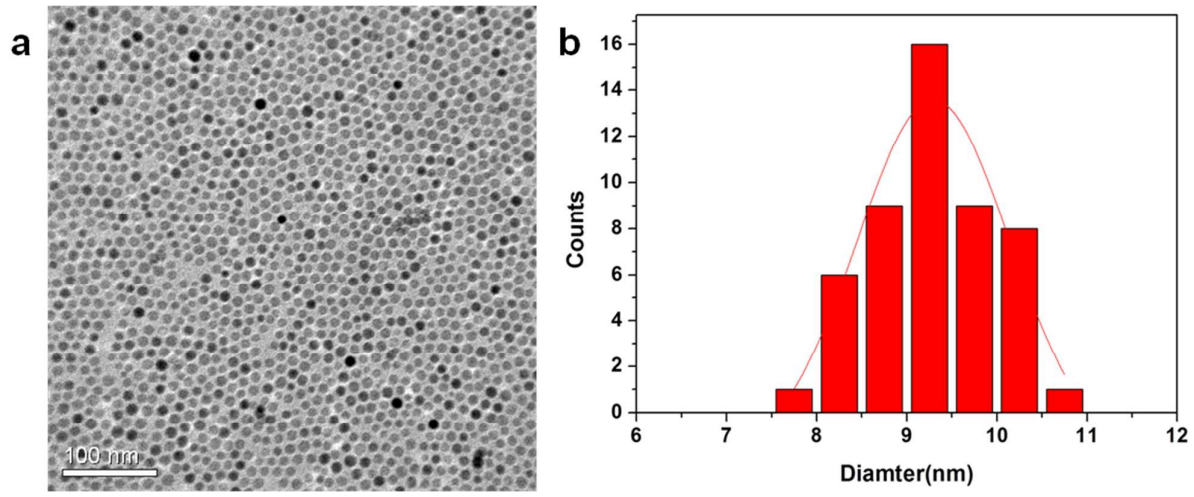

Figure S1. (a) Low magnification TEM image of Fe_3O_4 NPs (cf. high magnification TEM image shown in Figure 1a). (b) The corresponding histogram analysis (50 particles are used in this histogram). The average diameter of the NPs is 9.28±0.71nm

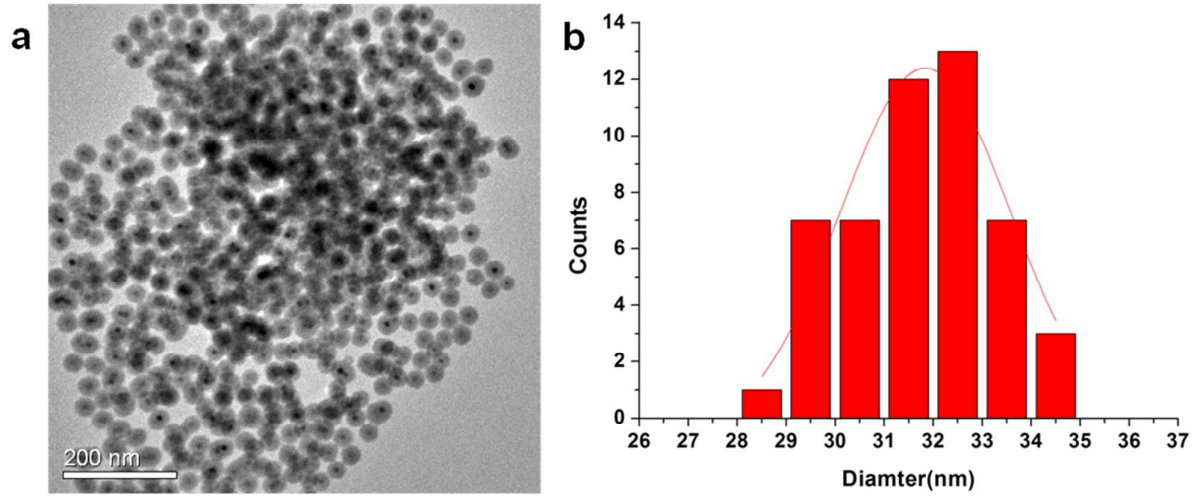

Figure S2. (a) Low magnification TEM image of Fe_3O_4@SiO_2(FITC) NPs (cf. high magnification TEM image shown in Figure 1b). (b) The corresponding histogram analysis (50 particles are used in this histogram). The average diameter of the NPs is 31.71±1.54nm

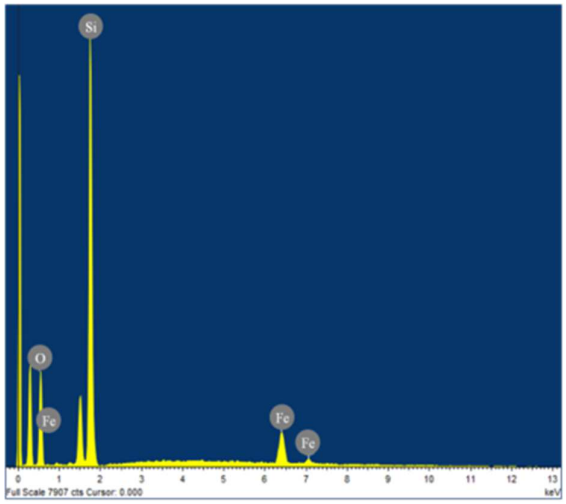

Figure S3. The energy-dispersive X-ray (EDX) spectra of Fe_3O_4@SiO_2(FITC) which confirms the existence of silicon, oxygen and iron elements

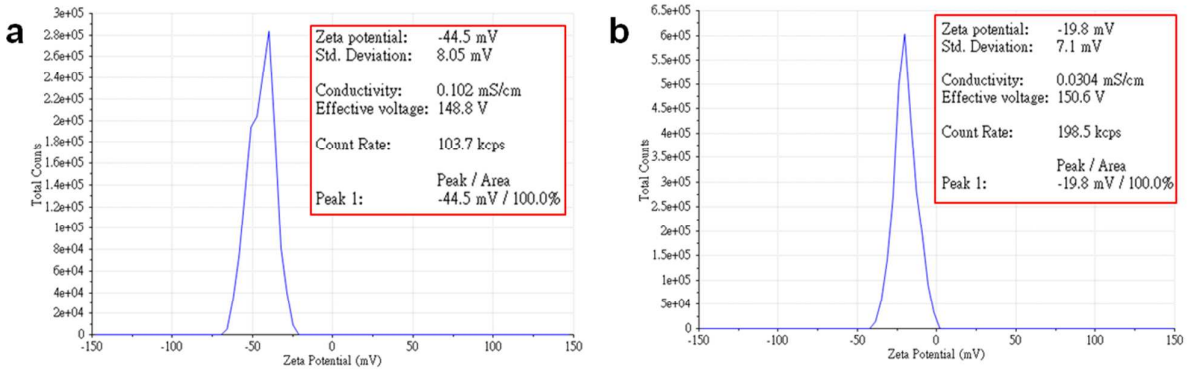

Figure S4. Zeta potential distribution shows the surface charge of (a) Fe_3O_4@SiO_2(FITC) and (b) Fe_3O_4@SiO_2(FITC)-NH_2

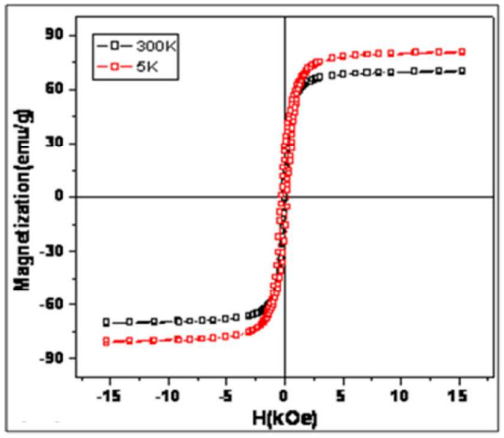

Figure S5. Field-dependent magnetization curves (at 5K and 300 K) of Fe_3O_4@SiO_2(FITC)-CD133

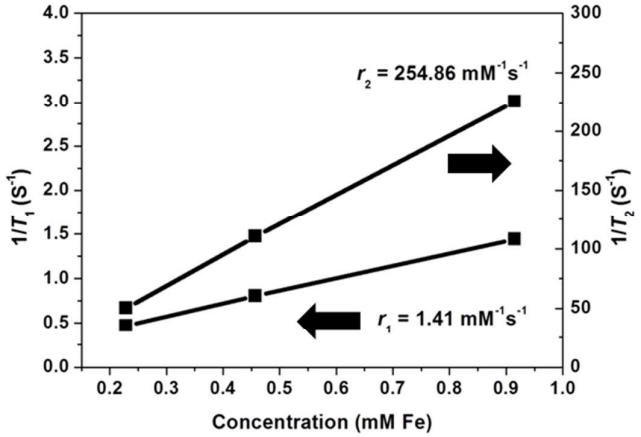

Figure S6. Relaxation property of Fe_3O_4@SiO_2(FITC)-CD133 at 0.47T

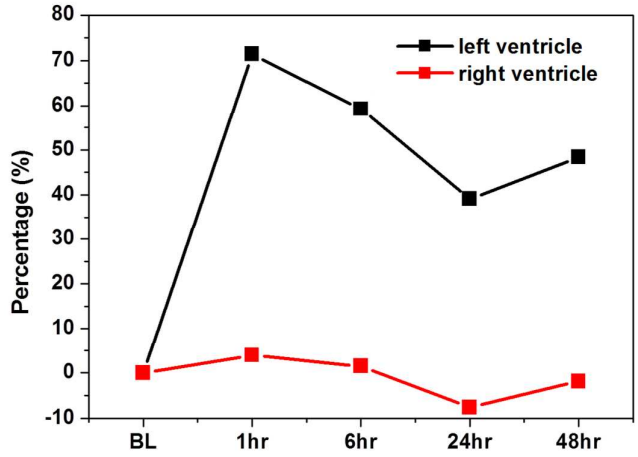

Figure S7. A time course T_2 signal of selected area in rat brain (row 3 in figure 3) at different time intervals